

Thermal radiative cooling of carbon cluster cations C_N^+ , $N = 9, 11, 12, 17 - 27$

Shimpei Iida,¹ Wei Hu,² Rui Zhang,² Piero Ferrari,³ Kei Masuhara,⁴ Hajime Tanuma,⁴ Haruo Shiromaru,⁴ Toshiyuki Azuma,⁵ and Klavs Hansen^{6,7,*}

¹*Tokyo Metropolitan University, Tokyo 192-0397, Japan*

²*School of Science, Tianjin University, 92 Weijin Road, Tianjin 300072, China*

³*Quantum Solid-State Physics, Department of Physics and Astronomy, KU Leuven, 3001 Leuven, Belgium*

⁴*Tokyo Metropolitan University, Tokyo 192-0397, Japan*

⁵*Atomic, Molecular and Optical Physics Laboratory, RIKEN, Saitama 351-0198, Japan*

⁶*Center for Joint Quantum Studies and Department of Physics,*

School of Science, Tianjin University, 92 Weijin Road, Tianjin 300072, China

⁷*Lanzhou Center for Theoretical Physics, Key Laboratory of Theoretical Physics of Gansu Province, Lanzhou University, Lanzhou, Gansu 730000, China*

(Dated: 2022-06-02, 00:49)

The radiative cooling rates of C_N^+ clusters ($N = 9, 11, 12, 17 - 27$) have been measured in the ultrahigh vacuum of an electrostatic storage ring to values on the order of 10^4 s^{-1} . The rates were measured as a competing channel to unimolecular decay, and the rate constants pertain to the excitation energies where these two channels compete. Such high values can only be explained as photon emission from thermally excited electronic states, a mechanism that has also been seen in polycyclic aromatic hydrocarbon cations. The high rates have a very strong stabilizing effect on the clusters and the underlying mechanism gives a high energy conversion efficiency, with the potential to reach high quantum efficiencies in the emission process. The competing decay of unimolecular fragmentation defines upper limits for photon energies that can be down-converted to lower energy photons. Including previously measured cluster sizes provides the limits for all clusters C_N^+ , $N = 8 - 27$, of values that vary from 10 to 14.5 eV, with a general increase with size. Clusters absorbing photons of energies below these limits cool down efficiently by emission of photons via electronic transitions and their fragmentation is strongly reduced, increasing their survival in HI regions.

INTRODUCTION

With the large and growing number of molecular species identified in interstellar space ([1, 2]), chemistry in vacuum is becoming increasingly important. A key question concerns the formation and survival of these molecules as well as the related question of the propensity for emission of photons from highly excited species.

The mechanisms by which internal excitation energy is dissipated play a crucial role for the survival rate of highly excited molecules and clusters and thereby also in the quantitative description of the abundances of carbon-containing compounds, such as clusters and in particular polycyclic aromatic hydrocarbon (PAH) molecules ([3–5]). In the virtually collision-free interstellar environment, dissipation of molecular excitation energy occurs overwhelmingly by unimolecular reactions or by radiative cooling, which makes studies of decays in ultrahigh vacuum storage rings and similar devices ideal for understanding such processes.

The radiative cooling from molecules in the interstellar medium has been discussed extensively in terms of various emission processes occurring in the infrared (e.g. [6]). An important alternative channel which is attracting increasing attention is photon emission from thermally populated electronic states.

For historical reasons, this mechanism is denoted recurrent fluorescence (RF). Also the term Poincaré radiation is used. RF does not require that the initial injection of excitation energy is a result of photon-absorption, although this excitation mode is expected to be common under interstellar conditions.

The energy released in the formation of molecules in collisional attachments may equally well provide the necessary excitation energy. The effect was suggested several decades ago ([7]) and in astrophysical context in [8, 9]. A number of laboratory experiments have already been interpreted in terms of this phenomenon, both for carbon containing species and for several metal and semiconductor clusters; see Refs. [10–15] for experiments on carbon anions. Of particular astrophysical interest are the applications where RF was invoked to explain the quenching of the decays of PAH molecules ([16–19]).

Studies of radiative cooling of several of the cationic carbon clusters in the homologous series reported here were given in [20]. Also the direct detection of photons emitted from size selected clusters in such processes has been accomplished with the observation of thermal, visible photons emitted from C_6^+ and C_4^+ ([21, 22]) and of naphthalene cations ([23]). Ref. [24] provides a review of the status of the laboratory studies of the subject until 2019. The recent report in [25] on the absorption spectra of carbon clusters corroborates the interpretation of the quenching as due to RF. The work reports absorption peaks of even-numbered cationic carbon clusters of sizes $n = 12 - 26, 28$ in the range from a little below 1 eV for the largest to a little above 2 eV for the smallest.

One astrophysical aspect of interest of these studies is the possibility of a connection to the extended red emission ([26–30]). Another is the still largely open question of the origin of the diffuse interstellar bands and their carriers ([31–33]), and the possible link to the carriers of the extended red emission ([34]).

The emission of RF photons occurs after excitation to quan-

tum states at energies that usually exceed thermal energies by a large factor, with a concomitant reduction in the populations of such excited states. The much higher oscillator strength of electronically excited states can nevertheless favor emission from these states over the slower photon emission via vibrational transitions. As a result, RF emission rates can reach values more than a factor thousand above those of infrared (IR) emission, making RF a highly competitive stabilizing channel for those molecules that exhibit the phenomenon, as well as an important source of photons in the near-IR and visible parts of the spectrum. The shortest measured time constants are those of metal clusters, but also carbon clusters can show very high photon emission rates, as demonstrated by the ten μs time constant observed for C_4^- ([13]) and the slightly longer values for cationic fullerenes ([35]).

The time constants of RF emission obviously depend strongly on the specific electronic structure of the radiating molecules via the energy of the excited and emitting state, and the observed values not surprisingly also vary widely. The most striking example of this chemical dependence is the radiative constants of small carbon anions. Both C_5^- and C_7^- radiate with time constants in the tens of ms range in vibrational transitions ([36, 37]), whereas both C_4^- and C_6^- have time constants around ten μs ([13, 14]). Equally striking is the effect of addition of a single hydrogen atom to C_6^- to form C_6H^- . This reduces the photon emission rate to values similar to those of C_5^- and C_7^- ([14]) and pentacene ([38]).

The measurements reported here were performed with an electrostatic storage ring. They made use of a special feature of most cluster sources that produce clusters or molecules in highly excited states, viz. that the energy distributions have widths that give rise to a wide continuum of rate constants. This continuum must then be considered in the description of the decay rates. In spite of the underlying statistical and completely exponential unimolecular decay rate constants, the measured decay rates, which are ensemble averages over these broad energy distributions, will for this reason give rise to non-exponential decay rates. Under reasonable general conditions these rates are well described by a power law, in the simplest form as $1/t$. The effect is well understood theoretically and has been discussed at length in the literature (see for example [39]) and documented experimentally (see [40] for the first experimental observation).

The simple power law requires that the experimentally detected unimolecular decay is the dominant energy loss channel. Photon emission will introduce an exponential suppression of the $1/t$ decay profile. The exponential suppression arises due to the different energy dependence of the two decays. A brief derivation is given below, and Ref. [24] can also be consulted for an analysis of this question. Specific examples of calculated rate constants for C_4^- and C_6^- , based on known spectroscopic and thermal properties of the clusters are given in [13, 41].

The exponential suppression of the power law decay can be used to determine quantitatively the radiative time constant ([10, 16, 42]). The radiative time constant measured is the

one pertaining to the energy where the two curves for the unimolecular decay and the photon emission cross (see Fig. 3 in [13] for an example). The measurements will give the quenching rate constant at this crossing energy with little need for any further characterization of the two decay rate constants involved. A majority of the determinations of the radiative rate constants in the references mentioned above has applied this technique. The determination of the energy content of the crossing point, however, requires an expression for the energy dependence of the unimolecular rate constant.

The experiments reported here measured the radiative quenching time for a number of cationic carbon clusters of medium size. They extend the measurements of the limited size range reported in [20] to a number of cluster sizes not previously produced in sufficient intensities to make the experiments feasible. For clusters C_{11}^+ and C_{19}^+ the measurements of spontaneous unimolecular decay quenching was supplemented by measurements of the decay rates induced by one-photon absorption at varying storage times, providing a test of the assumptions of a statistical decay and broad initial cluster energy distributions.

EXPERIMENTAL PROCEDURE

The clusters were produced in a laser ablation source by a 532 nm light pulse from a Nd:YAG laser hitting a rotating surface of graphite powder. The graphite feedstock was isotopically purified to ^{12}C , and all C_N^+ were mass-selected with sufficient resolution to separate $^{12}\text{C}_N^+$ from $^{12}\text{C}_N\text{H}^+$. No cooling gas was applied, and the ions were consequently produced highly excited with broad internal energy distributions. The source has previously been used for the production of a number of molecules and clusters with consistently reliable results for the width of the energy distribution, both for molecules desorbed intact and for clusters created during the ablation, as the clusters in the present study, and with both negative and positive charge. The relevant figure of merit in this context is the constancy and reproducibility of the time profiles of the spontaneous decays of the stored ions.

After production in the source, the ions were accelerated vertically to 15 keV, turned to horizontal motion and injected into the 7.7 m circumference storage ring, shown in Fig. 1, by switching the set of 10 degree deflection plates in the ring closest to the cluster source. All cations produced in the source were accelerated and injected into the ring. The cluster size of interest was selected by pulsing the set of 10 degree deflection plates closest to the injection gate twice. First time on injection and the second time when the different mass ions were spatially separated after a number of revolutions in the ring. Ref. [43] gives more details of this procedure and of the ring.

The decays were measured time-resolved turn-by-turn with a neutral particle detector. The detector hence monitored the quasi-instantaneous decay rate of the stored species, and *not* the surviving stored ion populations. The detector is located

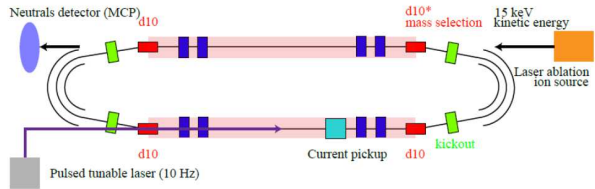


FIG. 1. A sketch of the electrostatic storage ring used in these studies, the TMU E-ring. The ions were produced in the laser ablation source shown in the upper right corner of the figure, accelerated to 15 keV and injected into the ring. The mass selection was accomplished by pulsing the potential on the 10 degree deflection plate d10* and on the kickout electrode. The neutral fragments that were produced during storage by decays in the top straight section were detected with the neutral particle detector at the end of that section on the top left of the figure. For the laser excitation experiments, a light pulse from a tunable Optical Parametric Oscillator (OPO) laser was introduced at the lower left hand corner with the light propagating toward the lower right corner along the straight section of the ring. After measurement, the ions were ejected by switching off the d10* deflection plates, which also prepared for the next injection.

at the end of the straight section of the injection side. An injection cycle ends with the ions being dumped after 90 or 10 ms of storage, depending on the decay rate, and a new cycle started.

The signal measured in the neutrals detector comprises all channels that emit neutral massive particles, irrespective of whether these are single atoms or molecules, and the measurements did not identify the decay product. The precise unimolecular decay channels are of interest for the energy content of the radiating clusters and the information on these channels available from the literature is therefore reviewed briefly in the discussion section.

The spontaneous decays were measured for cluster sizes $N = 9, 11, 12, 17 - 27$, and for laser enhanced decays also for $N = 11, 19$ (analogous results for $N = 8, 13 - 16$ were already reported in [20]). The number of ion injection cycles varied with size and reached 140 000 for $N = 27$ in order to reduce the statistical noise to a level comparable to or below the so-called betatron oscillations, which is the other main source of turn-by-turn fluctuations in the spectra.

Fig. 2 shows an example of the spontaneous decay rate of C_{11}^+ for the first few turns in the ring. The ions were injected in a short bunch and the turn-by-turn decays therefore appear as peaks, corresponding to the passage of the bunch through the detector side of the ring. The neutral counts seen in Fig. 2 up to $80 \mu\text{s}$ are decays of all species produced in the source and transferred to and stored in the ring before the final mass selection. The peaks seen between 25 and $70 \mu\text{s}$ are all from clusters separated by one carbon atomic mass. The mass selection pulse was applied around $80 \mu\text{s}$. Note that the spectrum

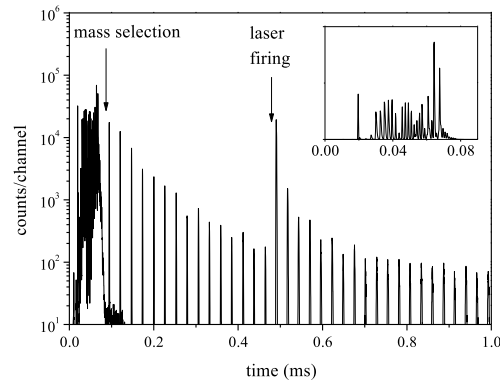


FIG. 2. The C_{11}^+ spontaneous and photo-induced decay rate after absorption of a 520 nm photon at the time indicated by the rightmost arrow. For these experiments a second detector located diagonally across from the primary was also used, and the circulation time is therefore twice the time separation of peaks seen in this figure.

represents decay rates and cannot be compared directly with spectra observed in mass spectrometers.

The figure also shows the enhanced counts caused by photo-excitation which here occurs just before 0.5 ms. Photo excitation was done with a single nanosecond pulse from a 10 Hz tunable optical parametrical oscillator laser. The wavelength was fixed at 520 nm (2.38 eV) and for $N = 19$ the laser was fired at times $9.7 + 10k$ ms, with k an integer from 0 to 7. For $N = 11$ the laser was fired at times 0.49, 1.02, 1.50, 2.02, 2.50, and 3.03 ms. The laser pulse energy was 1.0 mJ/pulse in all cases. The pulse energy was low enough to cause single photon absorption only.

RESULTS AND ANALYSIS

Fig. 3 shows spontaneous decay spectra of the clusters C_{20}^+ , C_{11}^+ , and C_{17}^+ with visibly different radiative cooling constants. After peak integration, the background induced by the collisions with the rest gas was subtracted. This was done by fitting an exponentially decreasing function to the measured signal at the last half of the storage time where the spontaneous decay had effectively ceased and only the collision-induced decay was present. Subtracting this background provided the spontaneous decay rates as a function of time.

In order to relate the observed decay rates to radiative cooling rate constants, we reiterate the derivation made in [13]. The measured signal, I_d , is proportional to the integral over the energy distribution of the product of the unimolecular rate constant and the population. For each energy, the latter is exponentially depleted by both the unimolecular decay and the photon emission, with the energy dependent rate constants, $k_d(E)$ and $k_p(E)$, respectively. Hence the measured unimolecular rate must be calculated as the integral (assuming a flat

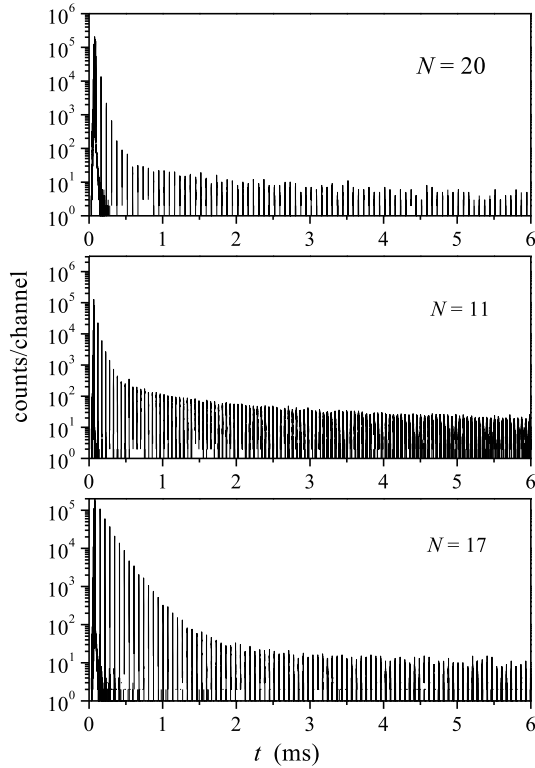


FIG. 3. The first six milliseconds of the measured spectra of, from top to bottom, C_{20}^+ , C_{11}^+ , and C_{17}^+ . The flat, almost constant parts of the spectra at the long times are due to rest gas collisions. The different cooling times are clearly seen as different cutoff times.

initial energy distribution):

$$I_d \propto \int_0^\infty k_d(E) e^{-(k_d(E) + k_p(E))t} dE. \quad (1)$$

The energy dependence of k_p is weak, in contrast to the very strong energy dependence of k_d . This is an effect of the fact that the frequency factor of the photon emission rate constant is limited by the Thomas-Reiche-Kuhn (TRK) sum rule and in practice is much smaller than that upper limit. This makes it many orders of magnitude smaller than that of the unimolecular decay. If photon emission is a competitive channel, this imposes the condition that also the ratio of the respective activation energies is significantly smaller than unity, i.e. that the photon energy is much smaller than the evaporative activation energy. These aspects are discussed in detail in [24]. With this general argument, the energy dependence of k_p can therefore be ignored compared to that of k_d and set to a constant in the integral, and the exponential containing it extracted from the integral:

$$I_d \propto e^{-k_p t} \int_0^\infty k_d(E) e^{-k_d(E)t} dE. \quad (2)$$

The integral is identical to that of the non-radiative decay rate. As calculated in several places, see e.g. [40], it is proportional to $1/t$ and hence

$$I_d \propto \frac{e^{-k_p t}}{t}. \quad (3)$$

For spontaneous decays, the time of ablation in the source is the zero of this time. In the laser excitation experiments, the absorption of the photon reheated the ions and thus restarted the power law decay with the laser firing time, t_{las} , as the redefined time zero. For small photon energies, the reheating may only be partial, as seen in [44]. However, fits of the photo-enhanced data with the equation

$$I_d \propto \frac{e^{-k_p t}}{t - t_{\text{las}}} \quad (4)$$

showed that absorption of the 520 nm photon effectively did reset the time to zero in these experiments.

The derivation sketched above requires that the emission of a single photon is sufficient to quench the unimolecular decay. This is the most likely scenario, given the electronic origin of the photons and the size of the clusters. The alternative is that the energy of the emitted photons is too low to quench the unimolecular decay. Then photon emission must instead best be described as continuous cooling. This will also produce an exponential suppression of the decay, albeit with a slightly different time dependence ([24]). In either case, the experimentally measured k_p is still the relevant quenching rate constant.

Proceeding with the assumption of large photon energies, the data have been fitted with the expression in equation (3) or equation (4), as applicable. To extract k_p , it is most convenient to rewrite the expressions as $\ln(I_d t)$ and $\ln(I_d(t - t_{\text{las}}))$ and fit a straight line. An example of such a fit is shown in Fig. 4, together with the semilog plot of the unmodified count rate for comparison. For the laser excitation experiments, the photo-enhanced signal was the relevant I_d . It was extracted from the data by subtracting a reference spectrum recorded without photo-excitation and normalized to identical intensity by the pre-laser counts.

The validity of the analysis requires that these photo-enhanced signals have the same values of the fitted k_p , independently of the storage time before photon absorption. These values should furthermore also be identical to those fitted from the spontaneous decays. The identical functional form of the decay curves for spontaneous and photo-enhanced signals for an initially flat energy distribution is intuitively clear: Single photon absorption shifts up the energy distribution by the photon energy, but for a flat distribution this does not change its shape, except for an overall multiplicative constant related to the product of laser fluence and photon absorption cross section. As the decay profile is determined by the underlying energy distribution, a flat energy distribution also does not change the measured decay rate, apart from the multiplicative constant and the shift in the zero of time to t_{las} .

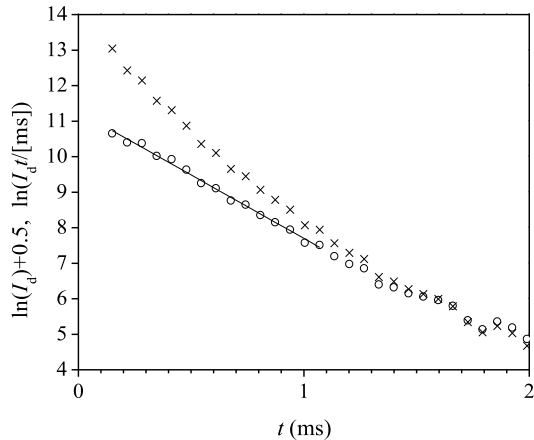


FIG. 4. The logarithm of the integrated peak intensity, I_d (crosses), and of the product tI_d (circles) for the spontaneous decay of the $N = 17$ cluster, chosen for its slow decay. The curvature on the I_d trace is clearly visible, whereas the tI_d trace shows the expected straight line behavior. The straight line is the fit of tI_d . The curves reach a noise floor at 10^{-3} of the initial signal a little above 2 ms. For display purposes $\ln(I_d)$ has been shifted up by 0.5.

Those requirements were tested previously in the study of the cationic carbon clusters of sizes reported in [20], but were also tested here with the laser excitation data recorded for C_{11}^+ and C_{19}^+ . Fig. 5 gives an example for C_{19}^+ . The figure shows identical slopes for the spontaneous decay and the decays at the earliest and latest laser firing times, as required for the analysis.

The fits for all storage times for both $N = 19$ and $N = 11$ are summarized in the averages shown in Fig. 6 which shows the values for all measured cluster sizes. For reference also those reported in Ref. [20] measured with the same storage ring and the same technique are given.

ENERGIES OF EMITTING CLUSTERS

The values of k_p provided by the analysis and shown in Fig. 6 are those for which the radiative rate constant is equal to the unimolecular decay rate constant,

$$k_p(E) \approx k_p = k_d(E_{\text{crossing}}), \quad (5)$$

where E_{crossing} is the energy at the curve crossing point, and the approximation consists of setting k_p to an energy independent value. The relation can be used to find the excitation energy of the clusters at this crossing point. These energies are also the upper limit of the energies for which the photon emission is the dominant decay channel. To a good approximation the decays are all radiative below this energy and fragmentation above.

The value of k_p in Eq.5 is the measured value. The dissociation rate constant, $k_d(E)$, is computed with the parameters

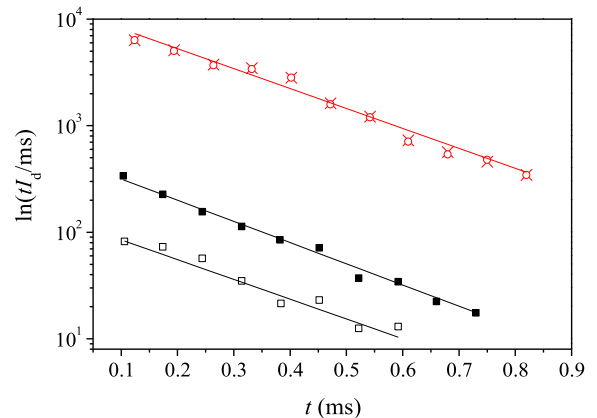


FIG. 5. Plots of $\ln(tI_d)$ vs. time for C_{19}^+ for spontaneous decays of a spectrum without laser excitation (red open circles) and the almost overlapping non-laser excited early time part of a laser-excited spectrum (red crosses); the photon enhanced decays for the laser firing times 10 ms (black filled squares) and for 80 ms (black open squares). The time zero for these two curves are their respective laser firing times. The point-by-point deviations from the straight line fits are mainly due to the betatron oscillations with an only very minor contribution from statistical fluctuations, demonstrating the reproducibility of the source.

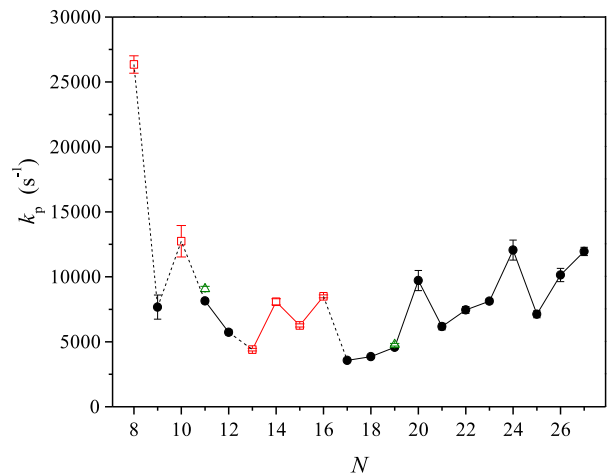


FIG. 6. All measured values of k_p , shown as filled black circles for the spontaneous decays, and for $N = 11$ and $N = 19$ as olive triangles for the values from the photo-excitation experiments. The clusters reported in [20] are shown as open red squares. Error bars are $1\text{-}\sigma$ values of the averages of the independently analyzed measurements of each cluster size.

given by a density functional theory (DFT) calculation which provides ground state energies and vibrational frequencies as well as the geometric structures. The calculations are performed with the ORCA 4.2.1 software package ([45]). The range-separated hybrid functional $\omega\text{B97X-D3}$ was employed ([46]), which also considers dispersion corrections ([47]). For the calculations, all the electrons of carbon were considered

implicitly, by the Def2-SVP basis set ([48]). This level of theory was selected in a previous study on C_N^+ clusters, where it was seen to correctly predict the transition from linear to cyclic conformers, at $N = 8$ ([20]). The calculations were conducted for $N = 9 - 27$, and for each of the cyclic and linear lowest-energy structures harmonic vibrational frequencies were calculated, which were always positive, confirming that the structures are minima and not saddle points.

The rate constant is calculated as the detailed balance value. The ground states of the clusters in this study are cyclic or possibly polycyclic for the larger sizes ([49]). We will proceed with the assumption that the monocyclic isomers represent all non-linear structures. The energies extracted from the decay dynamics derived in the following should be fairly insensitive to the precise number of rings in the clusters. Furthermore, we will assume that the linear and cyclic isomers interconvert freely, i.e. that the fragmentation decay is slower than these two rates.

The transition state is taken as the detachment of a trimer ([50]) from a linear isomer. With no activation barrier for the reverse process of attachment and taking into account rotational degrees of freedom by summation over the trimer angular momentum states, the expression reads ([51])

$$k_d(E) = \int_0^{E-D_{N,3}} d\epsilon \int_0^{E-D_{N,3}-\epsilon} d\epsilon_{\text{rot}} \omega(\epsilon) \frac{\rho_{N-3,3}^{(\ell)}(E-D_{N,3}-\epsilon-\epsilon_{\text{rot}})}{\rho_N^{(c)}(E)} \quad (6)$$

with $D_{N,3}$ the dissociation energy and

$$\omega(\epsilon) \equiv \rho_{3,\text{rot}}(\epsilon_{\text{rot}}) \frac{\sigma_{N-3,3} \mu_{N-3,3}}{\pi^2 \hbar^3} \epsilon. \quad (7)$$

The numerically most important single parameter in this expression is the dissociation energy which is the difference between the ground state energies of the cyclic C_N^+ and the dissociation products $C_{N-3}^+ + C_3$. It enters the energy argument of the level density of the decay product. The vibrational level densities, $\rho_{N-3,3}^{(\ell)}(E)$ and $\rho_N^{(c)}(E)$ for the products (linear) and for the reactant (cyclic), respectively, were calculated with the Beyer-Swinehart algorithm ([52]). $\rho_{N-3,3}^{(\ell)}(E)$ is calculated by pooling the vibrational frequencies of C_{N-3}^+ and C_3 . For the octamer, which is linear in the ground state and was measured in a previous experiment but also analyzed here, the equation is analogous, with the dissociation energy the linear-to-linear isomer value, and the cyclic isomer vibrational level density in the denominator replaced by that of the linear, $\rho^{(c)}(E) \rightarrow \rho^{(\ell)}(E)$.

The reverse process capture cross section is set to $\sigma_{\text{geo}} = 2\pi r_1^2 (1 + 3^{1/3})^2$, with $r_1 = 0.77 \text{ \AA}$, i.e. half the typical carbon-carbon bond length. The factor two represents the two possible attachment sites at each end of the linear cluster, and the remainder of the expression gives an estimate of the geometric size of the attachment cross section for each end of the chain. $\mu_{N-3,3}$ is the reduced mass of the channel, and $\rho_{3,\text{rot}}$ is the neutral trimer rotational level density. The two integrations were performed by direct summations of the discretized

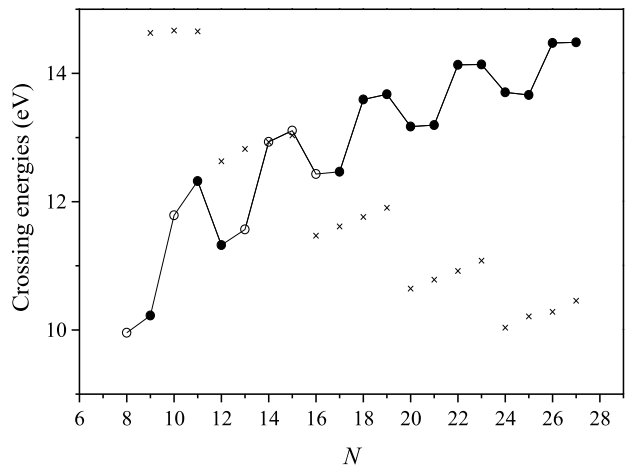


FIG. 7. Cooling thresholds for the measured clusters (filled symbols) and previously measured clusters (open symbols). The crosses give the second ionization energies determined with the DFT calculations described in the main text. The experimental uncertainties are less than the symbols size.

integrands over the kinetic energy released, ϵ , and the rotational energy ϵ_{rot} . For the trimer rotational states the quantum statistics of the rotational wave function was taken into account by using the symmetry number 2 and for the rotational constant the value $B = 0.4306 \text{ cm}^{-1} = 5.34 \times 10^{-5} \text{ eV}$ was used ([53]).

Fig. 7 shows the limits calculated when the experimentally measured values of k_p are set equal to equation (6), which is then solved for E . The period of four is due to periodic filling of the π electrons by addition of two electrons per carbon atom into four orbitals that are nearly degenerate. A significant contribution to the energies in Fig. 7 is the dissociation energies. As those also shape abundance spectra, the similarity of the curve seen here and the quartet structure in the abundances seen in spectra produced in hot sources ([54, 55]) is not an accident, although the precise connection between abundances and stability is more complicated than a simple one-to-one relationship ([51]). The general trend toward a higher energy for larger sizes is due in part to the kinetic shift, which in turn can be understood as due to the increase of the heat capacity with cluster size.

The figure also gives the second ionization energies calculated with the DFT software that was used for the other quantum chemical calculations in this work. The values are similar to the values reported in [56] for the smaller sizes where the two data sets overlap. The lowest of the two values for crossing energy and second ionization energy in the figure sets a limit to the photon energies that after absorption will be re-emitted as strongly redshifted photons. The cross-over energies in Fig. 7 exceed the second ionization energy of the largest species. This reduces the quantum efficiency for emission of lower energy photons for these species when photons with high energies are absorbed.

For a consideration of the complete picture it should be pointed out that absorption of above-threshold photons does not necessarily cause ionization. Instead clusters and molecules may absorb the photons and undergo intramolecular vibrational relaxation, opening up for RF photon emission after energy dissipation. Such non-ionizing photon absorption followed by relaxation has indeed been seen in C_{60} ([57]). The effect will cause the radiative cooling to be present also for photon energies above the second ionization threshold. The precise mechanism behind the effect is still unknown, both qualitatively and concerning the precise branching ratios. If active it will suppress a second ionization and raise the RF yield for carbon cation cluster sizes from $N = 16$ and up.

The derivation assumes that the photon emission rate constant is energy independent, and that the C_3 emission rate constant varies very rapidly at the point where the curves k_d and k_{ph} cross. We will now consider both these approximations.

A correction to the cross-over energy can be calculated in terms of the ratio of the photon energy ($h\nu$) and the evaporative activation energy (E_a) ([20]). It changes the cross-over time and hence implicitly the cross-over energy with the factor

$$\left(1 - \frac{h\nu}{E_a}\right). \quad (8)$$

This is small, and inverting the rate constant for this small time correction will result in an even smaller change in energy.

Secondly, the finite slopes of the two curves can potentially give rise to a smooth cross-over between the two channels as seen in [58]. The energy-specified photon emission branching ratio is given by the expression

$$R \equiv \frac{k_{ph}}{k_d + k_{ph}}. \quad (9)$$

The effect of finite values of the slopes of the two functions can be estimated by an expansion of the logarithm of the rate constant around the energy for which $R = 1/2$. We have to first order for a generic activated process

$$k(E + \delta E) \approx k(E) \exp\left(\delta E \frac{\partial \ln k}{\partial E}\right). \quad (10)$$

The derivative can be estimated from the energy dependence of an activated process. In analogy with the Van't Hoff equation, the logarithm can be written as

$$\ln k = c - E_a/T. \quad (11)$$

Taking the derivative with respect to energy gives

$$\frac{d \ln k}{dE} = \frac{E_a}{CT^2}, \quad (12)$$

where C is the heat capacity (k_B is set to unity). For the two parallel activated processes here, the relevant microcanonical temperatures are related approximately as ([59])

$$T_d = T - \frac{E_d}{2C}, \quad T_{ph} = T - \frac{h\nu}{2C}. \quad (13)$$

The channel-specific subtracted term is the leading order finite heat bath correction ([60]). As $h\nu < E_d$, the ratio of the derivatives is therefore bounded as

$$\frac{\frac{\partial \ln k_{ph}}{\partial E}}{\frac{\partial \ln k_d}{\partial E}} < \frac{h\nu}{E_d}. \quad (14)$$

The values of E_d account for the breaking of two bonds and vary between 9.5 and 12.7 eV. Reasonably, the photon energies are significantly smaller than that, and then we can obtain a good estimate of the energy by setting the derivative of the photon emission rate constant equal to a constant in the relevant region. Close to the expansion point $R = 1/2$ we then have the ratio

$$R \approx \frac{1}{1 + \exp\left(\delta E \frac{\partial \ln k_d}{\partial E}\right)}. \quad (15)$$

The derivatives are very high for all clusters in the study, with values between 30/eV and 38/eV for $N = 9 - 27$, and 110/eV for $N = 1$, making the cross-over region some tens of meV wide. For the lowest value of 30/eV, the branching ratio changes from 0.27 to 0.73 over the interval 0.066 eV.

The contrast to the very soft cross-over for anthracene found [58] is caused by the fact that for this molecule, both the derivative of the unimolecular reaction rate constant and the difference in the two derivatives are significantly smaller.

DISCUSSION

The experiment did not record the decay channel, apart from the fact that the detected fragment is neutral. It is still of some interest to know the moiety lost, however. Previous experiments with a range of different methods of production of the cations have established similar albeit not identical decay channels to those used here (the loss of C_3). The theory applied in the present work is in good agreement with the predominant channel seen in the photo-dissociation experiments in Ref. [50]. The pattern reported in [61] is as follows: Loss of C_1 for C_{11}^+ , C_{12}^+ , whereas C_{10}^+ and C_{16}^+ all lose C_3 , although for the latter this accounts for only half the yield and the remaining channels are emission of C_N , $N = 1, 2, 5$. Similar results were reported in [62]. High energy collisions give similar results up to the measured largest cluster $N = 10$, as reported in [63]. A study using collision induced dissociation showed C_5 as the main loss channels for C_{16}^+ and C_{19}^+ ([64]). In the isomer specific study in ([65]) on C_N^+ , $N = 7 - 10$, the authors also find branching ratios where loss of the neutral trimer is dominant for both linear and cyclic isomers, most strongly for the linear ones, and with other channels present for both types. The origin of the somewhat conflicting evidence from these previous experiments may partly be due to the different excitation procedures used.

In summary, the fragmentation losses appear to be predominantly of smaller molecules, larger than the monomer in the

majority of cases and with the trimer as the most dominant. We have disregarded this scattered information on the channels in our analysis, primarily because they do not have a strong influence on the crossing energies, which will be determined mainly by the dissociation energies, with an additional kinetic shift ([66]). The exact nature of the fragment emission channel nevertheless deserves clarification, as the lowest energy channel is what ultimately competes with photon emission. This clarification seems to be feasible with studies of delayed fragmentation in time-of-flight mass spectrometers, analogous to the procedure used in [67] to resolve a very similar question for silicon clusters.

The data given here have small statistical uncertainties. The main uncertainty is the assumptions associated with the description of the fragmentation precursor, i.e. statistical mixing and the values for the dissociation energies. Another uncertainty is the precise range of photon energies that will produce RF. This is of particular relevance in HI regions for $N \geq 16$ for which the second ionization potentials are below 13.6 eV, as non-ionizing absorption can give rise to thermally excited species even above threshold, and thus push the effective cross-over energy up. An interesting and connected side effect, which should be mentioned but will not be explored further here, is that absorption of high energy photons can also give rise to emission of low kinetic energy electrons, on the order of 1 eV ([57]).

Some other open questions remain for the clusters measured here. The most important is the spectrum of the emitted photons. The measured low temperature absorption spectra reported in Ref. ([25]) are likely to be smeared and possibly shifted at the high excitation energies of the clusters in the present study. This highly important question must be answered by future spectroscopic experiments. Those will also be needed to answer the question of precise values of quantum efficiencies and of the time scales needed to reach energies where the dominant emission occurs via vibrational transitions.

CONCLUSIONS

This study has determined the radiative cooling rate constants of a range of cationic clusters to be above 10^3 s^{-1} and for some above 10^4 s^{-1} . These cluster-specific constants define the time scales at which fragmentation is quenched and cooling occurs predominantly through photon emission. The values for the crossing energies for the largest studied clusters are higher than the photon energies available in HI regions ($h\nu < 13.6 \text{ eV}$) so these largest clusters are expected to be stable in these regions, except when multi-photon absorption occurs, cf. [3]. The energy at which this cross-over happens was calculated based on cluster properties given by a quantum chemical calculation and measured values for C_3 . This energy is significantly higher than any photon emitted. The infrared emission rate constants that are much smaller than the RF rates make that channel dominant only at correspond-

ingly lower excitation energies. This leaves a fairly wide energy window where energy loss occurs mainly by emission of visible and near-infrared photons, very likely with a resulting quantum efficiency above unity. Although open questions remain on the decay channels, the results reported here therefore give quantitative evidence for a mechanism that can provide a high yield of photons in the visible and NIR spectral range. Considering the difference in photon energies between the RF and IR photons and rates, the resulting RF energy dissipation rates for carbon cations at the crossing points are then higher than the infrared emission rate by three to four orders of magnitude.

The results pertain to the basic process of energy dissipation. It thus provides input to calculations such as those reported in [3], where the long term time development of molecular abundances is analyzed. The lifetime of clusters undergoing repeated cycles of photon absorption and emission depend, in addition to the absorption cross section, on both the ambient vacuum ultraviolet (VUV) light intensity and the rate of energy dissipation. The data here provide the first estimate of the difference in the fragmentation lifetimes of RF and IR dissipation. For the most conservative estimate of a two-photon absorption event required to cause fragmentation, and using the values 10^{-4} s and 10^{-2} s for the RF and IR time scales gives a factor 10^4 longer lifetimes. Clearly, the differences in radiative time scales of the two channels will have a corresponding impact on the limiting VUV flux for fragmentation.

Finally we note that the mechanism described here is present also for larger molecules, for example fullerenes, both for neutral but in particular for cationic species with their relatively high second ionization potential ([35]), as analyzed in [4] in connection with the fullerene formation mechanism. We also note that any excitation below the cross-over energy will give a quantum yield for RF photon emission of at least unity, because the first photon is emitted by that mechanism and the infrared cooling is far too weak to cause the rapid quenching. The precise quantum yield remains a subject of further study, though.

ACKNOWLEDGEMENTS

SI acknowledges the Grant-in-Aid for Early-Career Scientists (20K14386), and PF acknowledges the support of the Research Foundation - Flanders (FWO) with a postdoctoral grant. The computational resources and services used in this work were provided by the VSC (Flemish Supercomputer Center), funded by the Research Foundation - Flanders (FWO) and the Flemish Government. KH acknowledges funding from National Science Foundation of China (NSFC) with the grant 12047501 and the 111 Project under Grant No. B20063 from the Ministry of Science and Technology of People's Republic of China. Comments by A. Witt on astrophysical aspects and by T. Wakabayashi on carbon chemistry are gratefully acknowledged. Several constructive comments by

the reviewer are gratefully acknowledged.

DATA AVAILABILITY

The data underlying this article will be shared on reasonable request to the corresponding author.

* klavshansen@tju.edu.cn, hansen@lzu.edu.cn;
<http://www.klavshansen.cn/>

- [1] A. G. G. M. Tielens, *Rev. Mod. Phys.* **85**, 1021 (2013).
- [2] B. A. McGuire, *Astrophysical Journal Supplement Series* **239**, 1 (2018).
- [3] J. Montillaud, C. Joblin, and D. Toubanc, *A&A* **552**, A15 (2013).
- [4] O. Berné, J. Montillaud, and C. Joblin, *A&A* **577**, A133 (2015).
- [5] H. Andrews, A. Candian, and A. G. G. M. Tielens, *A&A* **595**, A23 (2016).
- [6] D. J. Hollenbach and A. G. G. M. Tielens, *Rev. Mod. Phys.* **71**, 173 (1999).
- [7] A. Nitzan and J. Jortner, *J. Chem. Phys.* **71**, 3524 (1979).
- [8] S. Leach, in *Polycyclic Aromatic Hydrocarbons and Astrophysics*, edited by A. Léger, L. d’Hendecourt, and N. Boccara (1987), vol. 191 of *NATO ASI Series*, pp. 99–127, ISBN 978-94-010-8619-6.
- [9] A. Léger, P. Boissel, and L. d’Hendecourt, *Phys. Rev. Lett.* **60**, 921 (1988).
- [10] J. U. Andersen, C. Brink, P. Hvelplund, M. O. Larsson, B. B. Nielsen, and H. Shen, *Phys. Rev. Lett.* **77**, 3991 (1996).
- [11] J. U. Andersen, C. Gottrup, K. Hansen, P. Hvelplund, and M. O. Larsson, *Eur. Phys. J. D* **17**, 189 (2001).
- [12] V. Chandrasekaran, B. Kafle, A. Prabhakaran, O. Heber, M. Rappaport, H. Rubinstein, D. Schwalm, Y. Toker, and D. Zajfman, *J. Phys. Chem. Lett.* **5**, 4078 (2014).
- [13] N. Kono, T. Furukawa, H. Tanuma, J. Matsumoto, H. Shiromaru, T. Azuma, K. Najafian, M. S. Pettersson, B. Dynefors, and K. Hansen, *Phys. Chem. Chem. Phys.* **17**, 24732 (2015).
- [14] G. Ito, T. Furukawa, H. Tanuma, J. Matsumoto, H. Shiromaru, T. Majima, M. Goto, T. Azuma, and K. Hansen, *Phys. Rev. Lett.* **112**, 183001 (2014).
- [15] N. Kono, R. Suzuki, T. Furukawa, J. Matsumoto, H. Tanuma, H. Shiromaru, T. Azuma, and K. Hansen, *Phys. Rev. A* **98**, 063434 (2018).
- [16] S. Martin, J. Bernard, R. Brédy, B. Concina, C. Joblin, M. Ji, C. Ortéga, and L. Chen, *Phys. Rev. Lett.* **110**, 063003 (2013).
- [17] J. Bernard, L. Chen, R. Brédy, M. Ji, C. Ortéga, J. Matsumoto, and S. Martin, *Nuc. Instrum. Meth. Phys. Res. B* **408**, 21 (2017).
- [18] S. Martin, L. Chen, A. Al-Mogeeth, and J. Bernard, *Phys. Rev. A* **99**, 012712 (2019).
- [19] M. H. Stockett, J. N. Bull, J. T. Buntine, E. Carrascosa, M. Ji, N. Kono, H. T. Schmidt, and H. Zettergren, *J. Chem. Phys.* **153**, 154303 (2020).
- [20] F.-Q. Chen, N. Kono, R. Suzuki, T. Furukawa, H. Tanuma, P. Ferrari, T. Azuma, H. Shiromaru, V. Zhaunerchyk, and K. Hansen, *Phys. Chem. Chem. Phys.* **21**, 1587 (2019).
- [21] Y. Ebara, T. Furukawa, J. Matsumoto, H. Tanuma, T. Azuma, H. Shiromaru, and K. Hansen, *Phys. Rev. Lett.* **117**, 133004 (2016).
- [22] M. Yoshida, T. Furukawa, J. Matsumoto, H. Tanuma, T. Azuma, H. Shiromaru, and K. Hansen, *J. Phys. Conf. Series* **875**, 012017 (2017).
- [23] M. Saito, H. Kubota, K. Yamasa, K. Suzuki, T. Majima, and H. Tsuchida, *Phys. Rev. A* **102**, 012820 (2020).
- [24] P. Ferrari, E. Janssens, P. Lievens, and K. Hansen, *Int. Rev. Phys. Chem.* **38**, 405 (2019).
- [25] J. Rademacher, E. S. Reedy, and E. K. Campbell, *J. Phys. Chem. A* **126**, 2127 (2022).
- [26] M. Cohen, C. M. Anderson, A. Cowley, G. V. Coyne, W. Fawley, T. R. Gull, E. A. Harlan, G. H. Herbig, F. Holden, H. S. Hudson, et al., *Astrophys. J.* **196**, 179 (1975).
- [27] G. D. Schmidt, M. Cohen, and B. Margon, *Astrophys. J.* **239**, L133 (1980).
- [28] D. G. Furton and A. N. Witt, *Astrophys. J. Lett.* **364**, L45 (1990).
- [29] D. G. Furton and A. N. Witt, *Astrophys. J.* **386**, 587 (1992).
- [30] A. N. Witt and T. S.-Y. Lai, *Astrophys. Space Sci.* **365:58** (2020).
- [31] F. Salama, G. A. Galazutdinov, J. Krellowski, L. Biennier, Y. Beletsky, and I.-O. Song, *Astrophys* **728**, 154 (2011).
- [32] A. Omont, *A&A* **590**, A52 (2016).
- [33] A. P. Jones, *R. Soc. open sci.* **3**, 160221 (2016).
- [34] T. S.-Y. Lai, A. N. Witt, C. Alvarez, and J. Cami, *MNRAS* **492**, 5853 (2020).
- [35] S. Tomita, J. U. Andersen, C. Gottrup, P. Hvelplund, and U. V. Pedersen, *Phys. Rev. Lett.* **87**, 073401 (2001).
- [36] M. Goto, A. E. K. Sundén, H. Shiromaru, J. Matsumoto, H. Tanuma, T. Azuma, and K. Hansen, *J. Chem. Phys.* **139**, 054306 (2013).
- [37] K. Najafian, M. S. Pettersson, B. Dynefors, H. Shiromaru, J. Matsumoto, H. Tanuma, T. Furukawa, T. Azuma, and K. Hansen, *J. Chem. Phys.* **140**, 104311 (2014).
- [38] S. Iida, S. Kuma, M. Kuriyama, T. Furukawa, M. Kusunoki, H. Tanuma, K. Hansen, H. Shiromaru, and T. Azuma, *Phys. Rev. A* **104**, 043114 (2021).
- [39] J. U. Andersen, E. Bonderup, and K. Hansen, *J. Phys. B* **35**, R1 (2002).
- [40] K. Hansen, J. U. Andersen, P. Hvelplund, S. P. Møller, U. V. Pedersen, and V. V. Petrunin, *Phys. Rev. Lett.* **87**, 123401 (2001).
- [41] V. Chandrasekaran, A. Prabhakaran, B. Kafle, H. Rubinstein, O. Heber, M. Rappaport, Y. Toker, and D. Zajfman, *J. Chem. Phys.* **146**, 094302 (2017).
- [42] K. Hansen and E. E. B. Campbell, *J. Chem. Phys.* **104**, 5012 (1996).
- [43] S. Jinno, T. Takao, K. Hanada, M. Goto, K. Okuno, H. Tanuma, T. Azuma, and H. Shiromaru, *Nuc. Instr. Methods Phys. Res. A* **572**, 568 (2007).
- [44] A. E. K. Sundén, M. Goto, J. Matsumoto, H. Shiromaru, H. Tanuma, T. Azuma, J. U. Andersen, S. E. Canton, and K. Hansen, *Phys. Rev. Lett.* **103**, 143001 (2009).
- [45] F. Neese, *WIREs Comput. Mol. Sci.* **8**, 1327 (2018).
- [46] Y.-S. Lin, J.-D. Li, S.-P. Mao, and J.-D. Chai, *J. Chem. Theory Comput.* **9**, 263 (2013).
- [47] S. Grimme, J. Antony, S. Ehrlich, and H. Krieg, *J. Chem. Phys.* **132**, 154104 (2010).
- [48] F. Weigend and R. Ahlrichs, *Phys. Chem. Chem. Phys.* **7**, 3297 (2005).
- [49] G. v. Helden, P. R. Kemper, N. G. Gotts, and M. T. Bowers, *Science* **259**, 1300 (1993).
- [50] M. E. Geusic, M. F. Jarrold, T. J. McIlrath, R. R. Freeman, and W. L. Brown, *J. Chem. Phys.* **86**, 3862 (1987).

- [51] K. Hansen, *Statistical Physics of Nanoparticles in the Gas Phase*, vol. 73 of *Springer Series on Atomic, Optical, and Plasma Physics* (Springer, Dordrecht, 2018), (2nd edition).
- [52] T. Beyer and D. F. Swinehart, *Commun. ACM* **16**, 379 (1973), ISSN 0001-0782.
- [53] C. A. Schmittenmaer, R. C. Cohen, N. Pugliano, J. R. Heath, A. L. Cooksy, K. L. Busarow, and R. J. Saykally, *Science* **1990**, 897 (1990).
- [54] P. Joyes and M. LeLeyter, *J. Phys.* **45**, 1681 (1984).
- [55] E. A. Rohlfing, D. M. Cox, and A. Kaldor, *J. Chem. Phys.* **81**, 3322 (1984),
- [56] S. Díaz-Tendero, G. Sánchez, P.-A. Hervieux, M. Alcamí, and F. Martín, *Brazilian Journal of Physics* **36**, 529 (2006).
- [57] K. Hansen, R. Richter, M. Alagia, S. Stranges, L. Schio, P. Salén, V. Yatsyna, R. Feifel, and V. Zhaunerchyk, *Phys. Rev. Lett.* **118**, 103001 (2017).
- [58] M. Ji, J. Bernard, L. Chen, C. Ortéga, A. Joblin, C. and Cassimi, and S. Martin, *J. Chem. Phys.* **146**, 44301 (2017).
- [59] J. U. Andersen, E. Bonderup, and K. Hansen, *J. Chem. Phys.* **114**, 6518 (2001).
- [60] C. E. Klots, *J. Chem. Phys.* **90**, 4470 (1989).
- [61] C. Lifshitz, T. Peres, and I. Agranat, *Int. J. Mass Spectrom. Ion Proc.* **93**, 149 (1989).
- [62] P. P. Radi, T. Bunn, P. Kemper, M. Molchan, and M. T. Bowers, *J. Chem. Phys.* **88**, 2809 (1988).
- [63] K. Béroff, M. Chabot, F. Mezdari, G. Martinet, T. Tuna, P. Désesquelles, A. LePabellec, and M. Barat, *Nuc. Instrum. Method Phys. Res. B* **267**, 866 (2009).
- [64] M. B. Sowa-Resat, P. A. Hintz, and S. L. Anderson, *J. Phys. Chem.* **99**, 10736 (1995).
- [65] K. Koyasu, T. Ohtaki, N. Hori, and F. Misaizu, *Chem. Phys. Lett.* **523**, 54 (2012).
- [66] C. Lifshitz, *Eur. J. Mass Spectrom.* **8**, 85 (2002).
- [67] P. Ferrari, E. Janssens, P. Lievens, and K. Hansen, *J. Chem. Phys.* **143**, 224313 (2015).